J Intell Robot Syst (2018) 89:107–119
DOI 10.1007/s10846-017-0472-2

Curved Path Following Control for Fixed-wing Unmanned Aerial Vehicles with Control Constraint

Shulong Zhao · Xiangke Wang · Daibing Zhang · Lincheng Shen

Received: 12 June 2016 / Accepted: 5 January 2017 / Published online: 21 January 2017

Abstract The control inputs of a fixed-wing unmanned aerial vehicle (UAV) are affected by external environment, the largest mechanical limits and energy limits. It is essential to consider the control constraints for the curved path following problem when the curvature of the desired path is continuing-changed. This paper presents two approaches to address the curved path following problem of fixed-wing UAVs subject to wind and we explicitly account for the control constraints. First, a proper state feedback controller is developed that is based on the tracking error equation defined in the Frenet-Serret frame to confirm that there is a control Lyapunov function (CLF) for input constrained case. Second, a stabilizing guidance law with control damping based on the designed CLF, which satisfies the small control property, is implemented to ensure the global asymptotic stability of the fixed-wing UAV curved path following subject to wind. Meanwhile, a control scheme with the nested saturation (NS) theory for curved path following is also developed with proven stability. The simulation results are presented to illustrate the effectiveness and high tracking performances of the proposed control strategies.

S. Zhao · X. Wang (✉) · D. Zhang · L. Shen
College of Mechanics and Automation,
National University of Defense Technology, Changsha, 410073, People's Republic of China
e-mail: xkwang@nudt.edu.cn

Keywords Curved path following · UAV · CLF · NS · Control constraint

Nomenclature

κ	curvature of the path
δ_1	along track error (m)
δ_2	cross tracking error (m)
$\tilde{\chi}$	error of the course angle (rad)
$\dot{s}$	velocity of the ghost vehicle (m/s)
ψ	the heading angle of the UAV (rad)
ψ_p	the path angle (rad)
χ	the course of the UAV (rad)
W	wind speed (m/s)
$p(x, y)$	position of the UAV (m)
V_a	the airspeed of the UAV (m/s)
V_g	the groundspeed of the UAV (m/s)
ω	the control input of the heading angle (rad/s)
$R(\psi_p)$	the rotation matrix from the Frenet-Serret frame to the inertial frame
ω_{max}	the maximum value of ω (rad/s)

1 Introduction

In recent decades, unmanned aerial vehicles (UAVs), which are equipped with cameras or other sensors, have been primarily used in numerous applications, such as forest fire monitoring, surveillance, photography and urban traffic managements. In general, these

missions can be implemented via remote control (RC) with limited links on the local scale. However, it is essential to employ a reliable and excellent autopilot for long or real-time missions. One important feature of an autopilot is that the UAV must move along a predefined path for these applications [13]. There are two types of algorithm to achieve the objective, as follows: (1) trajectory tracking and (2) path following. The main difference is that trajectory tracking requires the UAV to converge and follow a time-parameterized path [16]. It is noted in [20] that the trajectory tracking problem is not appropriate for a small fixed-wing UAV because of fuel inefficiency and the object is too rigorous to achieve, which may lead the vehicle to stall subject to wind.

For actual flight applications, first, we give some fixed waypoints (WPs) in space and then a proper reference path is planned to connect those WPs. The path following algorithm drives the vehicle to converge and follow a desired path, which is generally obtained via WPs with three forms: straight line, orbit and curve. The simplest path between two WPs is a straight line without any considered constraints. On the basis of the conclusion of Dubin [2], whether a desired path in two-dimensional plane is flyable or not is determined by the curvature of the desired path. The UAV must fly within its maximum bounds, and the curvature of the desired path is related to the lateral acceleration of the UAV. A curved segment of zero curvature ($\kappa = 0$) is a straight line and a curved segment of constant curvature ($\kappa = 1/R$) is an orbit. For the majority of applications, the desired path composed of straight lines and orbits is enough to complete the tasks [6, 11]. However, special missions require accurately following the curved path by turning smoothly, including aggressive maneuvers [1], flocking and formation [9], obstacle avoidance and passing through narrow spaces between buildings [3]. Meanwhile, if the desired path is the composition of the straight lines and orbits, it is impossible to achieve a smooth transition of curvature between two neighbour segments.

Park introduces a nonlinear guidance logic (NLGL) for fixed-wing UAV path following [15]. The centrifugal acceleration is adopted as the lateral acceleration, and a fixed distance from the UAV to the desired path is used to adjust the rate of convergence. This guidance law is simple and intuitive to implement in most commercial autopilots. The vector fieldv approach is utilized in the straight line and loiter path following problem [14], and this study is extended to the curved path in [8]. In this approach, the cross tracking error is defined as the distance from the UAV to the closest point on the path, which may result in a singularity when the closest points exceeded one. To overcome this drawback, Rysdyk proposes a guidance law that results in a constant line-of-sight (LOS) orientation relative to the UAV [10], and the notion of convergence to within a "tube" around the desired path. In addition, a nonlinear differential geometric three-dimensional (3D) path following guidance is proposed in [7], which introduces a differential geometry of curves that integrated an advanced vector to avoid the singularity.

Despite the potential applications of UAVs and the rich field experiences with the curved path following approaches, none of the previously cited works have taken the control constraints explicitly into account. Ren develops a constrained nonlinear tracking control strategy for small fixed-wing UAVs [17]. A set of all control constrained inputs that are suitable with respect to a proper control Lyapunov function (CLF) is constructed, and the guidance law is selected from this set. However, the design of an available set is complex, and the results are used for trajectory tracking for fixed-wing UAVs. Beard uses the nested saturation (NS) theory to convert control input constraints to command angle constraints [4]. In this work, the NS theory is employed to develop path following methods that roll, and flight path angle constraints are considered only for straight line and orbit.

Conventional fixed-wing UAVs have six-degree of freedom (positions and rotations) and four control surfaces (two ailerons, an elevator and a rudder). The control inputs of a vehicle are influenced by the external environment, the largest mechanical limits and energy limits, which must meet many control constraints, depending on its desired path and flight circumstances. Therefore, it is critical to consider these control constraints and convert them to state constraints (tracking error, airspeed, and flight angle) for the curved path following problem. Because the dynamic models of the small fixed-wing UAVs are not adequately accurate, it is unreliable to resolve these constraints via aerodynamic model approaches. Instead, we develop two control schemes to address curved path following problem using CLF and NS theory in the Frenet-Serret frame [12]. CLF is a valid tool for considering nonlinear problems because it can

provide a universal formula for constructing a stabilizing controller. The most important formula for obtaining a stabilizing controller that is based on an existing CLF was proposed in [19] and is known as Sontag's formula.

The outer-loop guidance control of a fixed-wing UAV is only considered here, and we assume that a proper inner-loop of the autopilot exists to implement low level commands in the vehicle. The main contributions of this study are summarized as follows.

1. A control scheme based on the CLF method is proposed for curved path following problem with input constraint. We developed a stabilizing guidance law based on the existing CLF with control damping to cancel out the oscillations in the control inputs within constraint, and the asymptotic stability of the closed loop is guaranteed and suitable control inputs are created within constraints.
2. A control scheme with the NS theory for fixed-wing UAV curved path following is developed, and the stability of the proposed control law is also proven. This scheme is an extension of the work of [4] to curved path.
3. A high-fidelity semi-physical simulation scheme is employed to illustrate the effectiveness and high tracking performances of the proposed control strategies and the control results were compared with the methods proposed in [5, 10, 14].

The rest of the paper is organized as follows. In Section 2, we summarize the primary introduction of the tracking error equation and some necessary notations. Then, we include a proper CLF for the tracking error system with the constrained case, and a suitable control strategy to satisfy the constraint conditions is explained in Section 3 . Simulation results are reported in Section 4 and some concluding remarks are presented in Section 5.

2 Background and Problem Statement

A planar model of the UAV is employed to perform a coordinated flight. In the field of path following, this model is extensively utilized and is suitable for describing the navigation kinematics of most commonly distributed fixed-wing UAVs, which are equipped with a propeller and a set of control surfaces.

The coordinate of the UAV is shown in Fig. 1. The position of the UAV is at (x, y), and the green dotted line represents the desired path. V_a and V_g are airspeed and groundspeed of the UAV, respectively. $W = (W_x, W_y)$ is the wind speed. ψ and χ are the heading angle and the course of the UAV, respectively. The heading angle is the direction in which the UAV is pointed. The course is the direction of travel relative to the Earth's surface. In the absence of wind and sideslip, the course angle is equal to the heading angle. Additionally, δ_1 and δ_2 denote the along tracking error and the cross tracking error, respectively. $\rho = \sqrt{\delta_1^2 + \delta_2^2}$ is the tracking error, and $\dot{s}$ can be regarded as the velocity of a ghost vehicle on the path, which is introduced as an additional control input. The path angle $\psi_p = \arctan 2(\dot{y}_p, \dot{x}_p)$.

The model of the UAV is adopted as follows [14]:

$$\begin{aligned} \dot{x} &= V_a \cos\psi + W_x \\ \dot{y} &= V_a \sin\psi + W_y \\ \dot{\psi} &= \omega \end{aligned} \tag{1}$$

where ω is the control input, i.e. the angular velocity of the heading angle.

For small fixed-wing UAVs, the wind speed often ranges from 20 % to 50 % of the airspeed. Figure 1

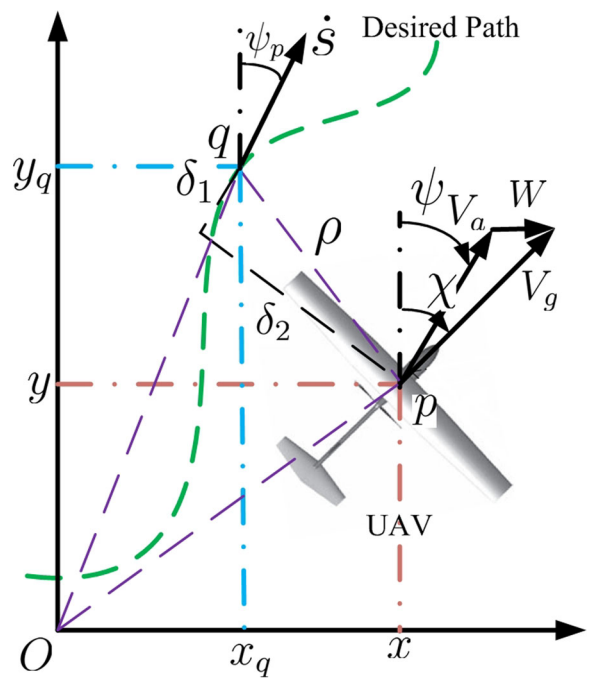

Fig. 1 Coordinate of the UAV

shows the wind triangle of the UAV, and the course χ is the angle between the projection of the ground velocity vector V_g onto the horizontal plane and the true north. Then, (1) can be equivalently expressed as

$$\begin{aligned} \dot{x} &= V_g \cos\chi \\ \dot{y} &= V_g \sin\chi \\ \dot{\chi} &= \Gamma(\psi)\omega \end{aligned} \tag{2}$$

where, $\Gamma(\psi) = \frac{V_a^2 + V_a(W_x\cos\psi + W_y\sin\psi)}{V_a^2 + W_x^2 + W_y^2 + 2V_a(W_x\cos\psi + W_y\sin\psi)}$.

We can obtain the error kinematic model of a fixed-wing UAV for the path following problem in the Frenet-Serret frame [18], as follows:

$$\begin{aligned} \dot{\delta}_1 &= V_g\cos\tilde{\chi} - (1-\kappa(s)\delta_2)\dot{s} \\ \dot{\delta}_2 &= V_g\sin\tilde{\chi} - \kappa(s)\delta_1\dot{s} \\ \dot{\tilde{\chi}} &= \Gamma(\psi)\omega - \kappa(s)\dot{s} \end{aligned} \tag{3}$$

Assumption 1 *The error of the course angle* $|\tilde{\chi}| = |\psi_p - \chi| \le \frac{\pi}{2}$ *and the error of the heading angle* $|\tilde{\psi}| = |\psi_p - \psi| \le \frac{\pi}{2}$.

Remark 1 The heading angle and course angle of the UAV are defined in $[-\pi, \pi]$. The objective of path following is that the nose of the UAV adjusts to the desired orientation as quickly as possible. Therefore, the error of the course angle or heading angle is defined in $[0, \pi]$. The error can be converted to $[-\pi/2, \pi/2]$ through selecting a reasonable origin. Then, it is clear that $|\tilde{\chi}| \le \frac{\pi}{2}$ and $|\tilde{\psi}| \le \frac{\pi}{2}$.

Remark 2 Denote the inertial position of the UAV by $p = [x, y]^T \in \mathbb{R}^2$. The inertial position of the point on the path associated with arc-length parameter s is denoted by $q(s) = [x_q(s), y_q(s)] \in \mathbb{R}^2$. The rotation matrix from the Frenet-Serret frame to the inertial frame is

$$R(\psi_p) = \begin{bmatrix} \cos\psi_p & -\sin\psi_p \\ \sin\psi_p & \cos\psi_p \end{bmatrix} \tag{4}$$

Then, we can obtain

$$[\delta_1, \delta_2]^T = R^T(\psi_p)(p - q(s)) \tag{5}$$

Our objective for the curved path following is that the fixed-wing UAV should be derived convergent to the predefined curved path in which the cross tracking error approaches zero and the heading angle of the UAV follows the path angle of the desired path. In Eq. 3, the control input is $u = [\omega, \dot{s}]^T$ where ω indicates the turning rate of the heading angle and $\dot{s}$ stands for the velocity of the ghost vehicle. The input constraint is presented as

$$U = \{\omega | -\omega_{max} < \omega < \omega_{max}\} \tag{6}$$

where, ω_{max} is the maximum value of ω.

3 Path Following Schemes

Here, we introduce the concepts of the CLF and the small control property. The global stabilization problems are addressed for fixed-wing UAVs curved path following using the CLF theory. Then, we extend the main results proposed in [17] to curved path and a control scheme using the NS theory is also developed for the curved path following problem with the control constraints.

3.1 CLF Method

We select $x_1 = \tilde{\chi}, x_2 = \delta_2, x_3 = \delta_1$, and (3) can be rewritten as

$$\begin{aligned} \dot{x}_1 &= u_0 - \kappa(s)u_1 \\ \dot{x}_2 &= V_g\sin x_1 - \kappa(s)x_3u_1 \\ \dot{x}_3 &= V_g\cos x_1 - (1-\kappa(s)x_2)u_1 \end{aligned} \tag{7}$$

where, $u_0 = \omega, u_1 = \dot{s}$ are the control inputs.

It was reported in [17] that a special situation may appear during the period when the vehicle tracks the desired path. If δ_1 and $\tilde{\chi}$ simultaneously go to zero, the second row of Eq. 3 will become $\dot{\delta}_2 = 0$. That is to say, δ_2 is uncontrollable at that moment. To avoid this special situation, we introduce a transfer $\hat{x}_1 = \lambda x_1 + x_2/\phi_1$, where $\phi_1 = \sqrt{1 + x_2^2 + x_3^2}$.

Then, we can obtain

$$\begin{aligned} \dot{\hat{x}}_1 &= \lambda(u_0 - \kappa(s)u_1) - \frac{\kappa(s)x_3u_1}{\phi_1} \\ &\quad + \frac{1+x_3^2}{\phi_1^3}V_g\sin\left(\frac{\hat{x}_1 - \frac{x_2}{\phi_1}}{\lambda}\right) - \frac{x_2x_3V_g\cos\left(\frac{\hat{x}_1 - \frac{x_2}{\phi_1}}{\lambda}\right) - u_1}{\phi_1^3} \\ \dot{x}_2 &= V_g\sin\left(\frac{\hat{x}_1 - \frac{x_2}{\phi_1}}{\lambda}\right) - \kappa(s)x_3u_1 \\ \dot{x}_3 &= V_g\cos\left(\frac{\hat{x}_1 - \frac{x_2}{\phi_1}}{\lambda}\right) - (1-\kappa(s)x_2)u_1 \end{aligned} \tag{8}$$

Equation 8 can be expressed in an affine nonlinear form, as follows:

$$\dot{x} = f(x) + g(x)u \tag{9}$$

where, $x = [\hat{x}_1, x_2, x_3]^T$, $u = [u_0, u_1]^T$,

$$f(x) = \begin{pmatrix} \frac{1+x_3^2}{\phi_1^3} V_g \sin(\frac{\hat{x}_1 - \frac{x_2}{\phi_1}}{\lambda}) - \frac{x_2 x_3}{\phi_1^3} V_g \cos(\frac{\hat{x}_1 - \frac{x_2}{\phi_1}}{\lambda}) \\ V_g \sin(\frac{\hat{x}_1 - \frac{x_2}{\phi_1}}{\lambda}) \\ V_g \cos(\frac{\hat{x}_1 - \frac{x_2}{\phi_1}}{\lambda}) \end{pmatrix} \tag{10}$$

$$g(x) = \begin{pmatrix} \lambda & -\lambda\kappa(s) - \frac{\kappa(s)x_3}{\phi_1} + \frac{1}{\phi_1^3} \\ 0 & \kappa(s)x_3 \\ 0 & 1 - \kappa(s)x_2 \end{pmatrix} \tag{11}$$

There are two steps in this control scheme. (i) A proper function V is devised, which is a CLF of system (9). (ii) According to the selected CLF, a control scheme is developed within the constraints.

Typically, it is not easy to design a proper CLF for a controlled system even though $f(x)$ and $g(x)$ are known because the stability of the closed loop is difficult to test [19]. Fortunately, there are many methods for the systematic construction of a proper CLF, such as the feedback linearizable method and strict feedback method. Here, we employ strict feedback method to develop the function V, and we confirm that V is also a CLF of Eq. 9.

Theorem 1 *For a curved path P in space, if the parameters are selected as $\lambda > 0$, $\lambda \neq \frac{1}{\kappa(s)\phi_1^3} - \frac{x_3}{\phi_1} + \frac{x_3}{\kappa(s)\hat{x}_1}$, $\lambda \neq \frac{1}{\phi_1^3\kappa(s)}$ and $0 < k_0 < \frac{2}{2+\lambda\pi}\omega_{max}$. The function*

$$V = \sqrt{1 + \hat{x_1^2} + x_2^2 + x_3^2} - 1 \tag{12}$$

is a CLF of the error system (9). Meanwhile, the feedback controller can be selected as

$$u_0 = -k_0\hat{x}_1 \tag{13}$$

$$u_1 = \begin{cases} V_g, & for \quad \hat{x}_1 = 0 \ and \ x_3 = 0 \\ -\frac{(3+4\phi_1)v}{2\eta_3\phi_1}, & otherwisee \end{cases}$$

within the constraint of U, where $\eta_3 = (-\lambda\kappa(s)\hat{x}_1 - \frac{\kappa(s)x_3}{\phi_1}\hat{x}_1 + \frac{\hat{x}_1}{\phi_1^3} + x_3)\frac{1}{\phi_2}$.

The proof of theorem 1 is presented in Appendix A.

Remark 3 The existing of the CLF for a controlled system is a commonly used assumption to guarantee that there is a controller to stabilize the system [19]. We introduce a proper CLF for the system (9) together with constraints. However, the feedback controller used in the proof is complex, and there are many limit conditions for the parameter selection. It is essential to develop a convenient and practical control scheme for the fixed-wing UAV curved path following.

Together with the feedback control, we provide the second result below.

Theorem 2 *The CLF for system (9) is considered. Then, the feedback control $u = [u_0, u_1]^T$ with*

$$u_i(x) = \begin{cases} -k_\gamma \mu_i(x) \frac{\gamma(x) + |\gamma(x)| + k_\mu \mu(x)}{\mu(x)}, & \mu(x) \neq 0 \\ 0, & \mu(x) = 0 \end{cases} \tag{14}$$

asymptotically stabilizes the controlled system (9), where, $i = 0, 1$, $\gamma(x) = L_f V(x)$, $\mu_i(x) = L_{g_i} V(x)$, g_i is the $i+1$th column of $g(x)$, $\mu(x) = \mu_0^2(x) + \mu_1^2(x)$. $k_\gamma > 1/2$, $k_\mu > 0$ are the parameters.

Proof Here, we proof the global asymptotic stability of control (14) for the closed loop system. The proof can be divided into two cases.

Case 1: $\mu(x) = 0$. According to the definition of the CLF, if $L_g V(x) = 0$ and $x \neq 0$, we obtain $L_f V(x) < 0$. Similarly, if $\mu(x) = 0$ and $x \neq 0$, we have $L_f V(x) < 0$. Thus, $\dot{V}(x) < 0$ satisfies the theorem.

Case 2: $\mu(x) \neq 0$. We calculate the derivative of $V(x)$ with the closed loop system

$$\begin{aligned} \dot{V}(x) &= L_f V(x) + L_g V(x) u \\ &= \gamma(x) - k_\gamma (L_g^0 V(x) u_0 + L_g^1 V(x) u_1) \\ &= \gamma(x) - k_\gamma (L_g^0 V(x) \mu_0(x) + L_g^1 V(x) \mu_1(x)) \\ &\quad \frac{\gamma(x) + |\gamma(x)| + k_\mu \mu(x)}{\mu(x)} \\ &= \gamma(x) - k_\gamma \frac{\gamma(x) + |\gamma(x)| + k_\mu \mu(x)}{\mu(x)} \mu(x) \\ &= (1 - k_\gamma)\gamma(x) - k_\gamma |\gamma(x)| - k_a k_\mu \mu(x) \end{aligned} \tag{15}$$

It is obvious that $(1 - k_\gamma)\gamma(x) - k_\gamma|\gamma(x)| < 0$ and $-k_\gamma k_\mu \mu(x) < 0$, and it follows $\dot{V}(x) < 0$. □

Remark 4 Here, we introduce the control parameter k_γ, which acts as control damping to cancel out oscillations of the control signal within constraints. The effect of this parameter is analyzed in the simulation.

3.2 NS Method

We also develop a control scheme with nested saturation theory for the fixed-wing UAV curved path following. This scheme can be regarded as an extension of the work of [4] for the curve path following.

Lemma 1 *(nested saturation)* [21] *A linear system that consists of multiple integrators is*

$$\dot{x}_1 = x_2, \ldots, \dot{x}_n = u \tag{16}$$

Linear functions h_i, exist for $i = 1, \ldots, n$ such that for a set of saturation functions σ_i with linear saturations (L_i, M_i), the saturation function is defined as

$$\sigma_{L_i,M_i}(x) = \begin{cases} L_i, & if \quad x \le L_i \\ x, & otherwise \\ M_i, & if \quad x \ge M_i \end{cases} \tag{17}$$

The control

$$u = -\sigma_n(h_n(x) + \sigma_{n-1}(h_{n-1}(x) + \ldots + \sigma_1(h_1(x)))) \tag{18}$$

results in a global asymptotic stability of the linear system.

Lemma 2 *For system (3), the control scheme for the curved path following is selected using the nest saturation theory*

$$\begin{aligned} \omega &= -\sigma_{M_1}\left(\frac{k_w z_1 + \sigma_{M_2}(k_z z_2)}{v\cos\tilde{\psi}}\right) \\ \dot{s} &= \frac{k_s z_1 + \sigma_{M_2}(k_z z_2)}{(\dot{\delta}_1 + v\cos\tilde{\psi})\kappa(s)} \end{aligned} \tag{19}$$

where, M_1 is a positive constant, $k_w > 0$, $k_s > 0$, $k_1 > 0$ and $k_z > 0$ are the control parameters. The variables z_1 and z_2 are defined as

$$\begin{aligned} \dot{z}_1 &= \ddot{\delta}_2 \\ \dot{z}_2 &= k_1\dot{\delta}_2 + \ddot{\delta}_2 \end{aligned} \tag{20}$$

Proof From system (3), we can obtain

$$\dot{z}_1 = \ddot{\delta}_2 = v\cos\tilde{\psi}\dot{\tilde{\psi}} - \kappa(s)\dot{\delta}_1\dot{s} \tag{21}$$

The Lyapunov function is selected as $V_1 = 1/2z_1^2$, and we calculate the derivative of V_1 as

$$\begin{aligned} \dot{V}_1 &= z_1\dot{z}_1 \\ &= z_1(v\cos\tilde{\psi}\dot{\tilde{\psi}} - \kappa(s)\dot{\delta}_1\dot{s}) \\ &= z_1 v\cos\tilde{\psi}\tilde{\omega} - z_1(\dot{\delta}_1 + v\cos\tilde{\psi})\kappa(s)\dot{s} \end{aligned} \tag{22}$$

The proof can be divided into two cases.

Case 1: $|z_1| \ge M_2/k_m, k_m = \min(k_w, k_s)$.

By substituting the control scheme (19) into (22)

$$\begin{aligned} \dot{V}_1 = &-z_1 v\cos\tilde{\psi}\sigma_{M_1}\left(\frac{k_w z_1 + \sigma_{M_2}(k_z z_2)}{v\cos\tilde{\psi}}\right) \\ &-z_1(\dot{\delta}_1 + v\cos\tilde{\psi})\kappa(s)\frac{k_s z_1 + \sigma_{M_2}(k_z z_2)}{(\dot{\delta}_1 + v\cos\tilde{\psi})\kappa(s)} \end{aligned} \tag{23}$$

With assumption 1, $|\tilde{\psi}| \le \frac{\pi}{2}$. Then, $\cos\tilde{\psi} \ge 0$. If $|z_1| \ge M_2/k_m$, we can obtain $sign(z_1) = sign(k_m z_1 + M_2)$, where $sign(\cdot)$ is a sign function. Because the saturation function σ_i is an odd function, it is clear that $\dot{V}_1 \le 0$.

Case 2: $|z_1| < M_2/k_m$.

If we can ensure that $|\frac{k_w z_1 + \sigma_{M_2}(k_z z_2)}{v\cos\tilde{\psi}}| \le M_1$, the saturation function will not reach the limit value. Then

$$\sigma_{M_1}\left(\frac{k_w z_1 + \sigma_{M_2}(k_z z_2)}{v\cos\tilde{\psi}}\right) = \frac{k_w z_1 + \sigma_{M_2}(k_z z_2)}{v\cos\tilde{\psi}} \tag{24}$$

Utilizing the Cauchy-Schwartz inequality,

$$\left|\frac{k_w z_1 + \sigma_{M_2}(k_z z_2)}{v\cos\tilde{\psi}}\right| \le \left|\frac{k_w|z_1| + M_2}{v\cos\tilde{\psi}}\right| \le \frac{2M_2}{v\cos\tilde{\psi}} \le M_1 \tag{25}$$

Equation 22 can be rewritten as

$$\dot{V}_1 = -z_1(k_w z_1 + \sigma_{M_2}(k_z z_2)) - z_1(k_s z_1 + \sigma_{M_2}(k_z z_2)) \tag{26}$$

We select $V_2 = 1/2z_2^2$ and calculate the derivative of V_2

$$\begin{aligned} \dot{V}_2 &= z_2\dot{z}_2 \\ &= z_2(k_1\dot{\delta}_2 + \ddot{\delta}_2) \\ &= z_2 k_1 z_1 - z_2(k_w + k_s)z_1 - 2z_2\sigma_{M_2}(k_z z_2) \end{aligned} \tag{27}$$

If we select parameter $k_1 = k_w + k_s$, then $\dot{V}_2 = -2z_2\sigma_{M_2}(k_z z_2) \le 0$, we can obtain $z_2 = k_1\delta_2 + \dot{\delta}_2 \to 0$. According to the input-to-state stability results, we can guarantee the state is $z_1 = \dot{\delta}_2 \to 0$ in Eq. 26. Therefore, $\delta_2 \to 0$ is guaranteed.

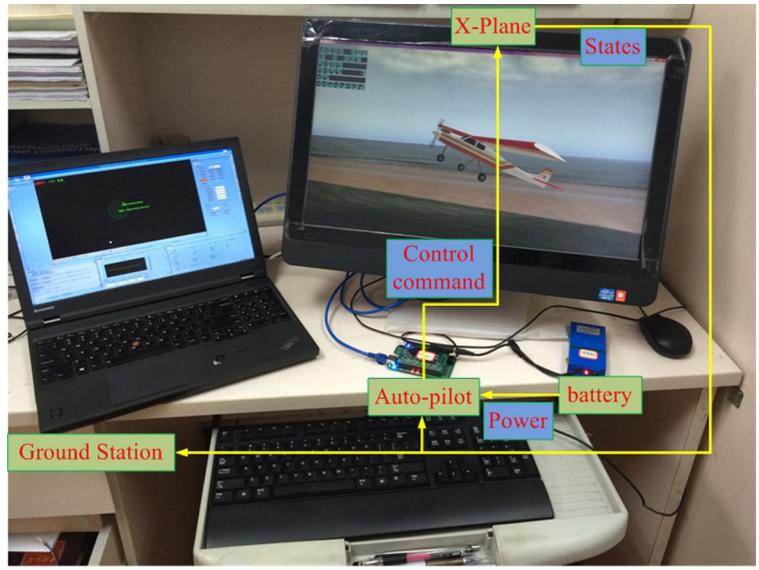

Fig. 2 High-fidelity semi-physical simulation environment, constructed by actual autopilot, ground station and X-Plane flight simulator

We also select $V_3 = 1/2\tilde{\psi}^2$ and calculate the derivative of V_3 as

$$\begin{aligned}\dot{V}_3 &= \tilde{\psi}\dot{\tilde{\psi}} \\ &= \tilde{\psi}(\tilde{\omega} - \kappa(s)\dot{s}) \\ &= -\tilde{\psi}\sigma_{M_1}\left(\frac{k_w z_1 + \sigma_{M_2}(k_z z_2)}{v\cos\tilde{\psi}}\right) - \tilde{\psi}\left(\frac{k_s z_1 + \sigma_{M_2}(k_z z_2)}{(\dot{\delta}_1 + v\cos\tilde{\psi})}\right)\end{aligned} \tag{28}$$

If we can ensure $\delta_2 \leq \frac{2v\cos\tilde{\psi}+\omega_2}{\kappa(s)\dot{s}} \leq \frac{2v\cos\tilde{\psi}_{max}+\omega_{2,max}}{\kappa(s)_{min}\dot{s}_{min}}$, then

$$\dot{\delta}_1 + v\cos\tilde{\psi} = 2v\cos\tilde{\psi} + \omega_2 - \kappa(s)\delta_2\dot{s} \geq 0 \tag{29}$$

Consider the following

$$k_w z_1 + \sigma_{M_2}(k_z z_2) = k_w(v\sin\tilde{\psi} - \kappa(s)\dot{s}\delta_1 + \omega_2) + \sigma_{M_2}(k_z z_2) \tag{30}$$

where $\dot{s}$ is the speed of the ghost vehicle, the maximum value of the gust wind is $\omega_{2,max}$. Then, we can guarantee that

$$|k_a v\sin\tilde{\psi}| > k_a\omega_{2,max} + M_2 - k_a M_3 > k_a\omega_{2,max} + M_2 - k_a\kappa(s)\delta_1\dot{s} \tag{31}$$

where, $k_a = \max(k_w, k_s)$, and $0 < M_3 < \kappa(s)\delta_1\dot{s}$. We will show that

$$|\sin\tilde{\psi}| > \frac{k_a\omega_{2,max} + M_2 - k_a M_3}{k_a v} \tag{32}$$

With assumption 1, $|\tilde{\psi}| \leq \pi/2$. The sin function in this interval is monotonously increased, which will guarantee that the sign of $\sin\tilde{\psi}$ and $k_a z_1 + \sigma_{M_2}(k_z z_2)$ are the same. Therefore, we can conclude that V_3 is definitely negative.

From Eqs. 25 and 32, we select $M_2 = M_1 v\cos\tilde{\psi}/2$, $\sin\tilde{\psi}_{max} = \frac{k_a\omega_{2,max}+M_2-k_a M_3}{k_a v}$.

Then, we can obtain

$$k_a v\sin\tilde{\psi}_{max} = k_a\omega_{2,max} - k_a M_3 + \frac{M_1 v}{2}\cos\tilde{\psi}_{max} \tag{33}$$

We solve this equation and obtain

$$\tilde{\psi}_{max} = \tan^{-1}\frac{M_1}{2k_a} + \sin^{-1}\frac{k_a\omega_{2,max} - k_a M_3}{v\sqrt{k_a^2 + M_1^2}} \tag{34}$$

Table 1 Positions of waypoints

Waypoint	WP1	WP2	WP3	WP4	WP5	WP6	WP7	WP8
Lon/deg	124.3159	124.3147	124.3206	124.3274	124.3248	124.3227	124.3203	124.3179
Lat/deg	48.2731	48.265	48.2614	48.265	48.2727	48.2712	48.2727	48.2712
x/m	0	−900.68	−1301	−900.71	−44.48	−211.27	−44.48	−211.27
y/m	0	88.81	−347.84	−851.14	−658.68	−503.27	−325.64	−148.02

Table 2 Parameters of the two control schemes

Parameter	Value	Parameter	Value
k_γ	0.9	k_μ	1
k_w	0.5	k_s	0.5
k_1	2	k_z	1
k_m	0.5	k_a	0.5
$\tilde{\psi}_{max}$	29.5 deg	$\delta_{2,max}$	$2/\kappa_{min}$
$\omega_{2,max}$	5 m/s	M_1	0.2 rad/s

Therefore, the value of the limit is given as

$$\delta_{2,max} = \frac{2v\cos\tilde{\psi}_{max} + \omega_{2,max}}{\kappa(s)_{min}\dot{s}_{min}} \tag{35}$$

$$\tilde{\psi}_{max} = \tan^{-1}\frac{M_1}{2k_a} + \sin^{-1}\frac{k_a\omega_{2,max} - k_aM_3}{v\sqrt{k_a^2 + M_1^2}}$$

□

4 Simulations and Discussions

To verify the performance of the path following schemes described in the previous sections, we developed a high-fidelity semi-physical simulation. The proposed approach is simulated with an X-plane environment, which provides very accurate aircraft models and has the possibility of exchanging data with external systems.

4.1 Simulation Platform

The entire system consists of three segments *a ground control station*, *an autopilot* and *an X-plane* as shown in Fig. 2. The ground control station is developed and employed to communicate with the X-plane using User Datagram Protocol communication. The autopilot and X-plane are connected with a network cable, which simulates a wireless transceiver. The X-plane provides all of the states of the UAV to the autopilot and simultaneously receives control commands. The ground control station is employed to record and present the flight procedure.

Throughout the simulation, X-plane is equivalent to the real UAV model and flight environment. X-plane is a high-performance simulation software, which can provide the closest to the real aircraft parameter model. The model in the X-plane is different from the one represented by the differential equation in the ordinary simulation. It not only contains all the parameters of the aircraft, but also has all the parameters generated by the interaction between the aircraft and the environment, so that the interference of the wind into the airplane can be added directly.

The autopilot in Fig. 2 is developed by our work group. The proposed curved path following schemes are implemented in the guidance loop of the autopilot and generate command to the low-level control loop. Together with the position, orientation, heading angle, and other information about the UAV to calculate the

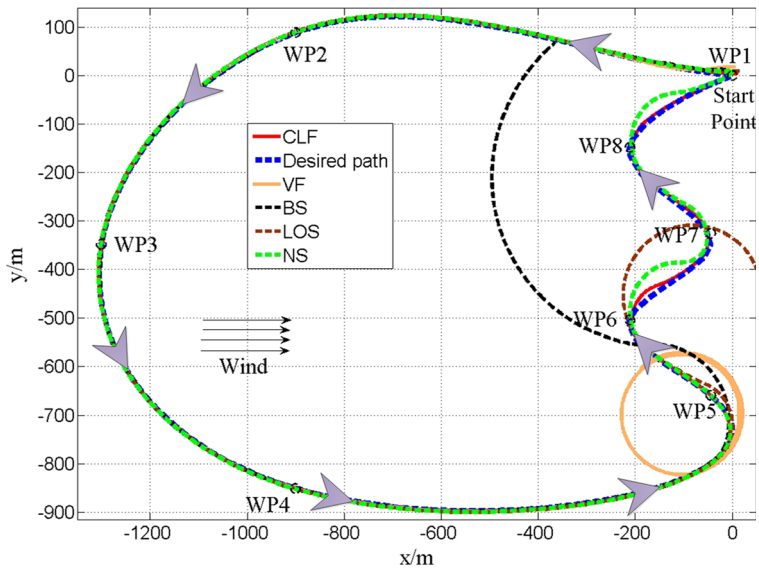

Fig. 3 Tracking results of different methods

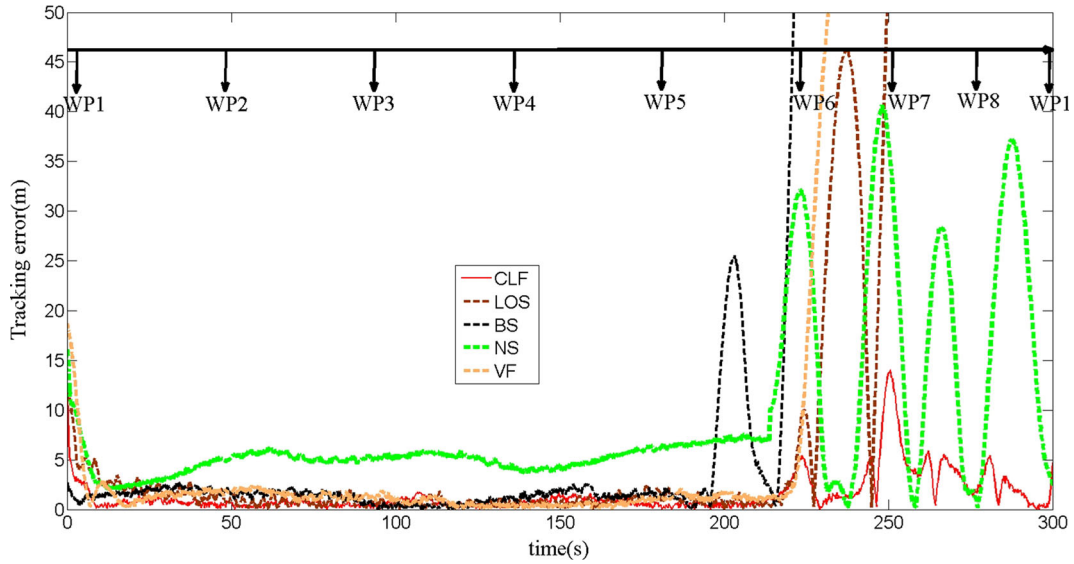

Fig. 4 Tracking errors of the CLF method and the NS method

low-level control signals in real time. We employ an active disturbance rejection control (ADRC) method to implement the inner-loop control, and the ADRC is proposed to address the nonlinear systems with uncertain dynamics and disturbances.

The *Great Planes PT-60 RC plane* is used in the simulations. Its main parameters include: a wing span is 1800 mm, the wing area is 58 dm^2, and the mass is 3180 g. The constraint of angle rate of this aircraft is 0.24 rad/s.

4.2 Simulation Results

Based on the distance, orientation and curvature, smooth curvature profiles can be easily provided. In actual flight applications, flight paths are determined by a

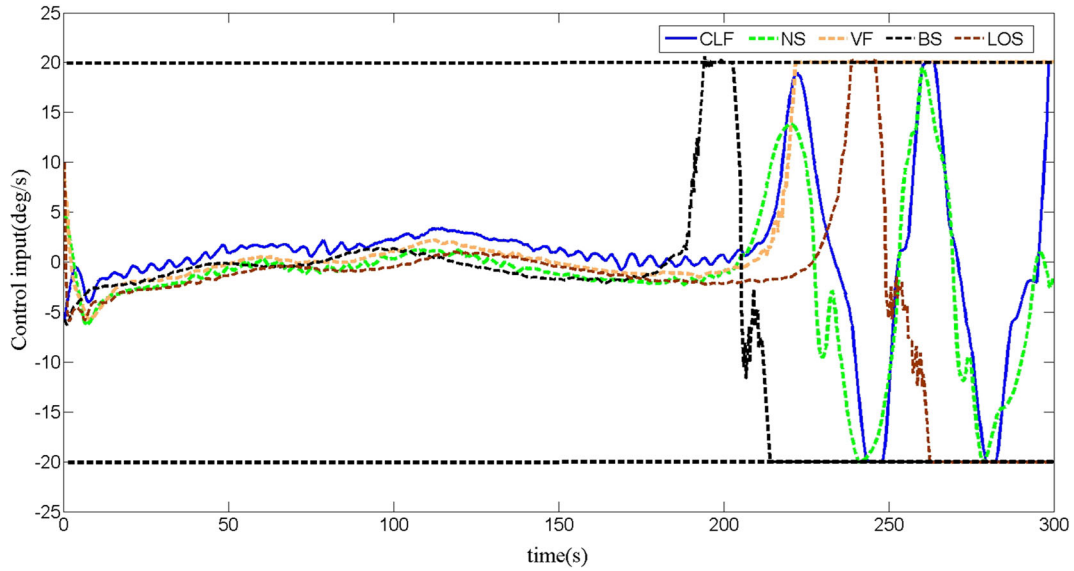

Fig. 5 Control inputs of the CLF method and the NS method

sequence of waypoints from the ground station. To obtain a continuous and non-constant curvature path, we employ a B-spline to produce paths that pass through predefined waypoints and a continuous curvature of paths. A B-spline curve $S : [0, 1] \rightarrow R^2$ is defined as

$$S(u) = \sum_{i=0}^{m} P_i N_{i,p}(u) \tag{36}$$

where, P_i is the control point and normalized path length parameter, u, is simply referred to as the path parameter. $N_{i,p}(u)$ is defined by the Cox-de Boor iterative formula

$$N_{i,0}(u) = \begin{cases} 1, & if \quad u_i \le u \le u_{i+1} \\ 0, & otherwise \end{cases} \tag{37}$$

$$Ni,\, p(u) = \frac{u-u_i}{u_{i+p}-u_i} N_{i,p-1}(u) + \frac{u_{i+p+1}-u}{u_{i+p+1}-u_{i+1}} N_{i+1,p-1}(u)$$

where u_i denotes knots, and $0 \le u_0 \le u_1 \le \cdots \le u_m \le 1$. The number of knots is $m + 1$, $U = [u_0, u_1, \ldots, u_m]$ is a knot vector, and p is the degree of the basic function. We define $p = 3$ in our simulations.

We select eight waypoints (in Table 1) to obtain the desired path, where the Lon and Lat represented the longitude and latitude, respectively.

The parameters in controller (14) and controller (19) that are selected are shown in Table 2.

To verify the effectiveness and applicability of the proposed methods with control constraints considered, we compare the tracking performances of the proposed CLF control method, NS control scheme, vector field (VF) method proposed in [14], adaptive backstepping (BS) method proposed in [5] and line-of-sight (LOS) method proposed in [10].

Constant airspeed of the UAV is 15 m/s. The wind speed ranges from 3 m/s to 7 m/s from 90 degrees southwest, which indicates that the wind speed accounts for 20 % to 50 % of the airspeed of the UAV. The results are shown in Fig. 3, which illustrates the ability of the proposed methods to follow a curved path with control constraints of control inputs (20 deg/s).

In the figure, the blue dashed curve represents the desired path and the red curve is the tracking path of the CLF method. The green curve stands for the tracking path of the NS method and the yellow curve indicates the performance of the VF method. The black curve stands for the tracking path of the BS method and the brown curve indicates the performance of the LOS method. When the desired curved path is benign (WP1-WP2-WP3-WP4-WP5), the tracking performance of the five methods are nearly no difference. When the curvature of the desired path is continuing-changed (WP5-WP6-WP7-WP8), VF, BS and LOS methods generate a sudden failure for the severe alteration of the curvature of the desired path without the control constraint considered. Since these methods do not have special considerations for input constraints, when the expected path is relatively gentle, the control is always within the limits. Therefore, the tracking effect is similar. When the expected path change is more intense, the control inputs of these three classical methods will enter the saturation limit, and method that there is no corresponding consideration will lead to tracking failure.

During this segment, an improvement in tracking performance of the CLF method is achieved with a reduced overshoot compared with the NS method. The tracking errors are shown in Fig. 4. In the figure, the range of tracking error over 50 m is negligible. The mean following errors on the curved path are 4.33 m and 15.46 m for the CLF method and the NS method, respectively. Thus, the tracking performance of the CLF method is better than the NS method with input constraints.

The control inputs of the two controllers are shown in Fig. 5. It is clear that method NS has larger oscillations than the CLF method because the only available information in the NS method during the simulation was the limits of command angle, which made it difficult to decrease the oscillations within the constraint. We find that when k_γ is very small, although the initial position of the UAV is close to the path, the oscillations of the control input are very large. However, if we choose a large k_γ, the oscillations of the control input become small and the problem of trajectory flattering arises because of the practical constants of the control. From the control input and tracking error of these five methods, we can find that once the UAV control input saturation and no corresponding processing strategy, the UAV will remain in the saturated state can not return to the normal tracking state.

5 Conclusion

In this paper, a novel control scheme using the control Lyapunov function (CLF) and a control scheme with the nested saturation (NS) theory are developed

to the curved path following problem of fixed-wing UAV with control constraints. The outputs of small fixed-wing UAVs are limited, and a certain turning time and turn radius are required. The problem of curved path following in the limited cases is different from that of ordinary path following, not only to ensure that the UAV converges to the desired curve path, but also to ensure that the control input is within the given range. If we do not specifically deal with the problem of limited input, when the curvature of the desired path is changing more dramatically, the UAV will deviate from the path or lead to tracking failure. The simulation results show that the proposed control schemes exhibit smooth and continuous effects under the arbitrary initial conditions and the tracking stages. In addition, the total energy consumptions should been addressed in the tracking law design, in order to prolong the flight time. In the further work, we will pay more attentions on the energy issues.

Acknowledgments This work is supported by National Natural Science Foundation (NNSF) of China under Grant 61403406.

Appendix A

Proof of theorem 1.

Proof It is clear that $V \geq 0$, and V is a continuously, differentiable and radially unbounded function.

We define $\phi_2 = \sqrt{1+\hat{x_1^2}+x_2^2+x_3^2}$, and

$$\frac{\partial V}{\partial x} \tag{38}$$

We also determined that

$$\begin{aligned}\frac{\partial V}{\partial x} f(x) = & \frac{v\sin(\frac{\hat{x}_1-\frac{x_2}{\phi_1}}{\lambda})}{\phi_2}(\frac{(1+x_3^2)\hat{x}_1}{\phi_1^3}+x_2) \\ & +\frac{v\cos(\frac{\hat{x}_1-\frac{x_2}{\phi_1}}{\lambda})}{\phi_2}(x_3-\frac{x_2x_3\hat{x}_1}{\phi_1^3})\end{aligned} \tag{39}$$

$$\frac{\partial V}{\partial x} g(x) = \begin{pmatrix} \frac{\lambda\hat{x}_1}{\phi_2} & (-\lambda\kappa(s)-\frac{\kappa(s)x_3}{\phi_1}+\frac{1}{\phi_1^3})\frac{\hat{x}_1}{\phi_2} \\ 0 & \frac{\kappa(s)x_3x_2}{\phi_2} \\ 0 & \frac{(1-\kappa(s)x_2)x_3}{\phi_2} \end{pmatrix} \tag{40}$$

By calculating $\frac{\partial V}{\partial x}\dot{x}$ directly

$$\begin{aligned}\frac{\partial V}{\partial x}\dot{x} &= [\frac{\hat{x}_1}{\phi_2}, \frac{x_2}{\phi_2}, \frac{x_3}{\phi_2}](f(x)+g(x)u) \\ &= (x_2+\frac{1+x_3^2}{\phi_1^2}\frac{\hat{x}_1}{\phi_1})\frac{1}{\phi_2}v\sin(\frac{\hat{x}_1-\frac{x_2}{\phi_1}}{\lambda}) \\ &\quad +(x_3-\frac{x_2x_3}{\phi_1^2}\frac{\hat{x}_1}{\phi_1})\frac{1}{\phi_2}v\cos(\frac{\hat{x}_1-\frac{x_2}{\phi_1}}{\lambda})+\lambda\hat{x}_1u_0\frac{1}{\phi_2} \\ &\quad +(-\lambda\kappa(s)\hat{x}_1-\frac{\kappa(s)x_3}{\phi_1}\hat{x}_1+\frac{\hat{x}_1}{\phi_1^3}+x_3)\frac{1}{\phi_2}u_1 \\ &= \eta_1+\eta_2+\eta_3u_1+\eta_4u_0\end{aligned} \tag{41}$$

where, $\eta_1 = (x_2+\frac{1+x_3^2}{\phi_1^2}\frac{\hat{x}_1}{\phi_1})\frac{1}{\phi_2}v\sin(\frac{\hat{x}_1-\frac{x_2}{\phi_1}}{\lambda})$,

$\eta_2 = (x_3-\frac{x_2x_3}{\phi_1^2}\frac{\hat{x}_1}{\phi_1})\frac{1}{\phi_2}v\cos(\frac{\hat{x}_1-\frac{x_2}{\phi_1}}{\lambda})$,

$\eta_3 = (-\lambda\kappa(s)\hat{x}_1-\frac{\kappa(s)x_3}{\phi_1}\hat{x}_1+\frac{\hat{x}_1}{\phi_1^3}+x_3)\frac{1}{\phi_2}$,

$\eta_4 = \lambda\hat{x}_1\frac{1}{\phi_2}$.

Utilizing the Cauchy-Schwartz inequality, we determined that

$$\begin{aligned}|\eta_1| &= |x_2+\frac{1+x_3^2}{\phi_1^2}\frac{\hat{x}_1}{\phi_1}||\frac{1}{\phi_2}|v|\sin(\frac{\hat{x}_1-\frac{x_2}{\phi_1}}{\lambda})| \\ &\leq |x_2+\frac{1+x_3^2}{\phi_1^2}\frac{\hat{x}_1}{\phi_1}||\frac{1}{\phi_2}|v \\ &\leq (\frac{|x_2|}{\phi_2}+|\frac{1+x_3^2}{\phi_1^2}||\frac{\hat{x}_1}{\phi_2}||\frac{1}{\phi_1})|v \\ |\eta_2| &= (x_3-\frac{x_2x_3}{\phi_1^2}\frac{\hat{x}_1}{\phi_1})\frac{1}{\phi_2}v\cos(\frac{\hat{x}_1-\frac{x_2}{\phi_1}}{\lambda}) \\ &\leq |(x_3-\frac{x_2x_3}{\phi_1^2}\frac{\hat{x}_1}{\phi_1})\frac{1}{\phi_2}|v \\ &\leq (\frac{|x_3|}{\phi_2}+|\frac{x_2x_3}{\phi_1^2}|\frac{|\hat{x}_1|}{\phi_2})\frac{1}{\phi_1}|)v\end{aligned} \tag{42}$$

Because $\phi_1^2 = x_2^2+x_3^2+1$, it is obvious that $|\frac{1+x_3^2}{\phi_1^2}| \leq 1$ and $|\frac{x_2x_3}{\phi_1^2}| \leq \frac{1}{2}$. According to the definition of ϕ_2, the inequalities of $\frac{|x_3|}{\phi_2} \leq 1$, $\frac{|x_2|}{\phi_2} \leq 1$ and $\frac{|\hat{x}_1|}{\phi_2} \leq 1$ are established. Then, we can obtain

$$|\eta_1| \leq (\frac{|x_2|}{\phi_2}+|\frac{1+x_3^2}{\phi_1^2}||\frac{\hat{x}_1}{\phi_2}||\frac{1}{\phi_1})|v \leq (1+\frac{1}{\phi_1})v \tag{43}$$

$$|\eta_2| \leq (\frac{|x_3|}{\phi_2}+|\frac{x_2x_3}{\phi_1^2}|\frac{|\hat{x}_1|}{\phi_2})\frac{1}{\phi_1}|)v \leq (1+\frac{1}{2\phi_1})v \tag{44}$$

By substituting (13) into (41), four cases are considered with respect to $\hat{x}_1$ and x_3.

Case 1: $\hat{x}_1 = 0$ and $x_3 \neq 0$.

We know that $\eta_3 = \frac{x_3}{\phi_2} \neq 0$, and $u_1 = -\frac{(3+4\phi_1)v}{2\eta_3\phi_1}$, then

$$\begin{aligned}\frac{\partial V}{\partial x}\dot{x} &= \eta_1 + \eta_2 + \eta_3 u_1 + \eta_4 u_0 \\ &= \eta_1 + \eta_2 - \frac{(3+4\phi_1)v}{2\phi_1} - \lambda k_0 \frac{\hat{x_1^2}}{\phi_2} \leq -\lambda k_0 \frac{\hat{x_1^2}}{\phi_2} \leq 0\end{aligned} \tag{45}$$

Case 2: $\hat{x}_1 = 0$ and $x_3 = 0$.

We know that $\eta_3 = 0$, $\eta_2 = 0$, and $u_1 = v$, then

$$\frac{\partial V}{\partial x}\dot{x} = \eta_1 + \eta_2 + \eta_3 u_1 + \eta_4 u_0 = \frac{x_2}{\phi_2} v \sin(-\frac{x_2}{\phi_1 \lambda}) - \lambda k_0 \frac{\hat{x_1^2}}{\phi_2} \tag{46}$$

Because the function $\sin(\cdot)$ is an odd function, it is clear that $x \sin(x)$ is semi-positive. Then we can conclude that

$$\frac{\partial V}{\partial x}\dot{x} \leq -\lambda k_0 \frac{\hat{x_1^2}}{\phi_2} \leq 0 \tag{47}$$

Case 3: $\hat{x}_1 \neq 0$ and $x_3 = 0$.

Because $\lambda \neq \frac{1}{\phi_1^3 \kappa(s)}$, it is obvious that $\eta_3 \neq 0$. The result is same to case 1.

Case 4: $\hat{x}_1 \neq 0$ and $x_3 \neq 0$.

For most situations, the result of case 4 is the same as in case 1. A special singular point is presented when $\lambda = \frac{1}{\kappa(s)\phi_1^3} - \frac{x_3}{\phi_1} + \frac{x_3}{\kappa(s)\hat{x}_1}$. According to the condition of λ, we can conclude that $\frac{\partial V}{\partial x}\dot{x} \leq 0$.

Using assumption 1, we can obtain $|x_1| \leq \frac{\pi}{2}$. Then

$$|\hat{x}_1| = |\lambda x_1 + \frac{x_2}{\phi_1}| \leq |\lambda x_1| + |\frac{x_2}{\phi_1}| \leq 1 + \frac{\pi\lambda}{2} \tag{48}$$

The control input u_0 is selected with (12), and together with the range of k_0

$$|u_0| \leq k_0 |\hat{x}_1| \leq k_0 (\frac{2+\pi\lambda}{2}) \leq \omega_{max} \tag{49}$$

thus completing the proof. □

References

1. Aguiar, A.P., Hespanha, J.P., Kokotović, P.V.: Performance limitations in reference tracking and path following for nonlinear systems. Automatica **44**(3), 598–610 (2008)
2. Amin, J.N., Boskovic, J.D., Mehra, R.K.: A fast and efficient approach to path planning for unmanned vehicles. In: Proceedings of AIAA Guidance, Navigation, and Control Conference and Exhibit, pp. 21–24 (2006)
3. Beard, R.W., Kingston, D., Quigley, M., Snyder, D., Christiansen, R., Johnson, W., McLain, T., Goodrich, M.: Autonomous vehicle technologies for small fixed-wing uavs. J. Aerosp. Comput. Inf. Commun. **2**(1), 92–108 (2005)
4. Beard, R.W., Ferrin, J., Humpherys, J.: Fixed wing uav path following in wind with input constraints. IEEE Trans. Control Syst. Technol. **22**(6), 2103–2117 (2014)
5. Brezoescu, A., Espinoza, T., Castillo, P., Lozano, R.: Adaptive trajectory following for a fixed-wing uav in presence of crosswind. J. Intell. Robot. Syst. **69**(1-4), 257–271 (2013)
6. Chao, H., Cao, Y., Chen, Y.: Autopilots for small fixed-wing unmanned air vehicles: A survey. In: 2007 International Conference on Mechatronics and Automation, pp. 3144–3149. IEEE (2007)
7. Cho, N., Kim, Y., Park, S.: Three-dimensional nonlinear differential geometric path-following guidance law. J. Guid. Control. Dyn. **38**(12), 2366–2385 (2015)
8. Griffiths, S.R.: Vector Field Approach for Curved Path Following for Miniature Aerial Vehicles. In: Proceedings of the AIAA Guidance, Navigation, and Control Conference vol. 61, pp. 63–64 (2006)
9. Lan, Y., Yan, G., Lin, Z.: Synthesis of distributed control of coordinated path following based on hybrid approach. IEEE Trans. Autom. Control **56**(5), 1170–1175 (2011)
10. Lekkas, A.M., Fossen, T.I.: Integral los path following for curved paths based on a monotone cubic hermite spline parametrization. IEEE Trans. Control Syst. Technol. **22**(6), 2287–2301 (2014)
11. Leven, S., Zufferey, J.C., Floreano, D.: A minimalist control strategy for small uavs. In: 2009 IEEE/RSJ International Conference on Intelligent RObots and Systems, pp. 2873–2878. IEEE, LIS-CONF-2009-007 (2009)
12. Lin, Z., Francis, B., Maggiore, M.: Necessary and sufficient graphical conditions for formation control of unicycles. IEEE Trans. Autom. Control **50**(1), 121–127 (2005)
13. Modirrousta, A., Khodabandeh, M.: A novel nonlinear hybrid controller design for an uncertain quadrotor with disturbances. Aerosp. Sci. Technol. **45**, 294–308 (2015)
14. Nelson, D.R., Barber, D.B., McLain, T.W., Beard, R.W.: Vector field path following for miniature air vehicles. IEEE Trans. Robot. **23**(3), 519–529 (2007)
15. Park, S., Deyst, J., How, J.P.: A new nonlinear guidance logic for trajectory tracking. In: AIAA guidance, navigation, and control conference and exhibit, pp. 16–19 (2004)
16. Ratnoo, A., Hayoun, S.Y., Granot, A., Shima, T.: Path following using trajectory shaping guidance. J. Guid. Control. Dyn. **38**(1), 106–116 (2014)
17. Ren, W., Beard, R.W.: Trajectory tracking for unmanned air vehicles with velocity and heading rate constraints. IEEE Trans. Control Syst. Technol. **12**(5), 706–716 (2004)
18. Rucco, A., Aguiar, A.P., Hauser, J.: Trajectory Optimization for Constrained Uavs: a Virtual Target Vehicle Approach. In: International Conference on Unmanned Aircraft Systems (ICUAS), vol. 2015, pp. 236–245. IEEE (2015)

19. Sontag, E.D.: A 'universal'construction of artstein's theorem on nonlinear stabilization. Syst. Control Lett. **13**(2), 117–123 (1989)
20. Sujit, P., Saripalli, S., Sousa, J.B.: Unmanned aerial vehicle path following: a survey and analysis of algorithms for fixed-wing unmanned aerial vehicless. IEEE Control. Syst. **34**(1), 42–59 (2014)
21. Teel, A.R.: Global stabilization and restricted tracking for multiple integrators with bounded controls. Syst. Control Lett. **18**(3), 165–171 (1992)

Shulong Zhao received the B.S. and M.S. degrees from Beihang University, China in 2011, and National University of Defense Technology, China in 2013, respectively. Currently he is a Ph.D. candidate of National University of Defense Technology. His research interests include data driven control, and curved path following of UAV.

Xiangke Wang received the B.S., M.S., and Ph.D. degrees from National University of Defense Technology, China, in 2004, 2006 and 2012, respectively. From 2012, he is with College of Mechatronic Engineering and Automation, National University of Defense Technology, China, and currently he is an associate professor there. His current research interests include coordination control of multiple UAV, nonlinear control of UAV.

Daibing Zhang received the B.S., M.S., and Ph.D. degrees from National University of Defense Technology, China, in 1999, 2002 and 2007, respectively. From 2007, he is with College of Mechatronic Engineering and Automation, National University of Defense Technology, China, and currently he is an associate professor there. His current research interests include multiple-rotor VTOL, flocking and formation control of UAVs, and nonlinear control of UAV.

Lincheng Shen received the B.E., M.S., and Ph.D. degrees in automatic control from the National University of Defense Technology, respectively. Since 1989, he has been with the Department of Automatic Control, where he is currently a Full Professor and serves as the Dean of the College of Mechatronics and Automation. He has published more than 100 technical papers in refereed international journals and academic conferences proceedings. His research interests include mission planning, autonomous and cooperative control for unmanned systems, biomimetic robotics, and intelligent control. He has been serving as an Editorial Board Member of the Journal of Bionic Engineering since 2007. He has initiated and organized several workshops and symposia, including the international workshop on bionic engineering (IWBE2012) and Chinese Automation Congress (CAC2013).